

Uncommon turbine architectures for distributed power generation – development of a small velocity compounded radial re-entry turbine

ANDREAS PAUL WEISS^{a*}
PHILIPP STREIT^a
TOBIAS POPP^a
PATRICK SHOEMAKER^b
THOMAS HILDEBRANDT^b
VÁCLAV NOVOTNÝ^c
JAN ŠPALE^c

Technical University of Applied Sciences Amberg–Weiden, Centre of Excellence for Cogeneration Technologies, Kaiser-Wilhelm-Ring 23, 92224 Amberg, Germany

^bNUMECA Ingenieurbüro Altdorf, Türkeistraße 11, 90518 Altdorf bei Nürnberg Germany

Czech Technical University in Prague, University Centre for Energy Efficient Buildings, Třinecká 1024, 273 43 Buštěhrad, Czech Republic

Abstract The energy industry is undergoing a major upheaval. In Germany, for example, the large nuclear and coal-fired power plants in the gigawatt scale are planned to be shut down in the forthcoming years. Electricity is to be generated in many small units in a decentralized, renewable and environmentally friendly manner. The large 1000 MW multistage axial steam turbines used to this date are no longer suitable for these tasks. For this reason, the authors examine turbine architectures that are known *per se* but have fallen into oblivion due to their inferior efficiency and upcoming electric drives about 100 year ago. However, these uncommon turbine concepts could be suitable for small to micro scale distributed power plants using thermodynamic cycles, which use for example geothermal wells or waste heat from industry to generate electricity close to the consumers. Thus, the

paper describes and discusses the concept of a velocity-compounded single wheel re-entry cantilever turbine in comparison with other turbine concepts, especially other velocity-compounded turbines like the Curtis-type. Furthermore, the authors describe the design considerations, which led to a specific design of a 5 kW air turbine demonstrator, which was later manufactured and investigated. Finally, first numerical as well as experimental results are presented, compared and critically discussed with regards to the originally defined design approach.

Keywords: Turbine; Radial, Re-entry; Velocity compounded

1 Introduction

The Rankine cycle with steam or organic vapors has been used for electricity generation for about 150 years. In the beginning, steam engines drove the generators but they were quickly substituted by the upcoming steam turbines, which allowed a by far higher power output per unit. At the end of the 20th century, the standard size of a coal-fired or a nuclear steam power plant was about one gigawatt, applying a multistage axial turbine as high-efficient expander. However, nowadays some countries like Germany give up nuclear power production and decided to stop electricity production based on coal in order to reduce environment pollution and to slow down the climate change. Alternative heat sources like geothermal heat, solar radiation or even waste heat from, e.g. industry processes shall be used to generate electricity in by far smaller units, close to the consumers. Small Rankine power stations below the megawatt-class or even below 100 kW are considered, e.g. in residential areas.

It is not reasonable regarding efficiency and specific costs to scale down the mentioned multistage axial turbine concept for shaft power of 1 MW or even only 100 kW. Other concepts for the turbo expander must be considered in order to be cost-effective. Therefore, the authors have started to investigate theoretically, numerically and experimentally other, rather uncommon turbine architectures like, e.g. cantilever quasi-impulse turbines

[1] or the velocity compounded radial re-entry turbine, which is the objective of the present paper. Some basic turbine physics will be repeated in the following in order to work out the pros and cons of such a design.

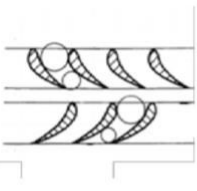
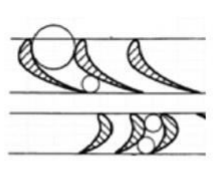
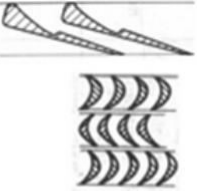
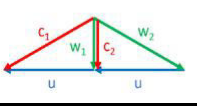
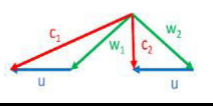
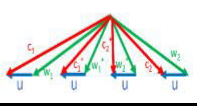
The first commercial steam turbine of de Laval was a single stage axial impulse turbine [2]. There is no pressure drop across the wheel (i.e. the buckets) in such an impulse turbine. Therefore, the nozzles convert the entire stage enthalpy drop, Δh_{is} , into a high absolute velocity, i.e. high

Mach number. Due to the combination with the rather low circumferential speed, u , the buckets have to perform a high deflection of the flow [3]. Therefore, the efficiency potential is only about 80% (see Table 1). Parsons introduced a so called reaction stage in which the stage enthalpy drop is equally distributed between nozzles and buckets [4]. Therefore, the maximum velocities, Mach numbers and flow deflections are smaller and the efficiency potential is about 90%. However, the reaction stage needs an $\sqrt{2}$

2 times higher circumferential speed for the same stage enthalpy drop as the impulse stage (compare [3]). Furthermore, partial admission cannot be used with a reaction turbine due to its pressure drop across the buckets. Partial admission is a mandatory measure to implement turbines with very small power output (i.e. mass flow rate) without getting too short blades or without needing a too high rotational speed, n , due to a very small turbine wheel diameter D . The last well-known turbine concept is the velocity compounded Curtis stage which was very popular in North America in the beginning of the 20th century [5]. The nozzles and the first wheel might be considered to be identical to the described impulse stage, however, the main difference is the required circumferential speed, which is only half of that of the impulse stage. Thus, after the vapor has passed the first wheel, it still contains 25% of the kinetic energy originally provided by the nozzles. A row of stator blades turns the flow back to the circumferential direction and guides it into the second wheel. The buckets of the second wheel convert the remaining kinetic energy into shaft power. The Curtis stage can also be used with partial admission. In combination with the necessary very low circumferential speed, it is predestined for small and simpler (cheaper) power output turbo expanders. However, its efficiency potential is with about 70% the smallest due to the highest relative Mach numbers, the highest flow deflections (see Table 1) and the huge wetted surface per stage. Although the Curtis stage was replaced in the 20th century by multistage reaction (Parsons) or multistage impulse (Rateau) turbines in big power stations, thanks to their higher efficiency potential, this concept has been still usable and valuable for highly loaded, high specific power turbines needed, e.g., for the turbo pumps of rocket engines [6, 7].

The turbo generator in a small-scale power station (< 100 kW) must be very simple, robust (like for a rocket turbo pump) and cost-effective. The authors describe in a former paper [8] that the single stage axial impulse turbine fulfills most of these requirements satisfactorily in small-scale ORC plants. However, if steam should be the working fluid, boundary conditions

Table 1: Comparison of different turbine concepts and their velocity triangles for the same stage enthalpy drop Δh_{is} .

Turbine type	Reaction turbine	Impulse turbine	Curtis turbine (2 wheels)
			
Velocity triangles			
U_{opt}	$(\Delta h_{is})^{0.5}$	$\frac{h}{2}$ 0.5	$\frac{1}{2} \frac{\Delta h}{2}$ 0.5
	141%	100%	50%
Partial admission	not feasible	feasible	feasible
Efficiency potential	90%	80%	70%

get even more challenging. Steam provides an order of magnitude higher enthalpy drop for a given heat source and heat sink temperature compared to organic fluids [9]. As a result, the mass flow rate or volume flow rate for a required shaft power is an order of magnitude smaller. Both factors result in a very low specific speed of the necessary turbine, what suggests a simple multistage design like, e.g. the discussed Curtis stage as an alternative. However, the simple and cost-effective architecture of a single turbine wheel, directly mounted on the shaft of the high-speed generator, avoiding a clutch, any additional bearing or sealings [8] should not be sacrificed with respect to specific costs. A solution could be a radial Curtis stage like introduced by, e.g. [10] or a radial re-entry cantilever turbine, a so called 'Elektra turbine' (see [11]), which is investigated for micro-applications in the present paper.

Figure 1 displays an Elektra-turbine out of [11], which consists of two Laval nozzles, a big diameter cantilever wheel and twice three flow deflection channels which force the steam to pass the buckets three times. Thus, a kind of a velocity compounded Curtis turbine can be implemented with just one wheel. The degree of admission of the first pass must be rather small ($< 10\%$) because the steam jet passes the wheel several times at different circumferential positions. The flow deflecting channels between two

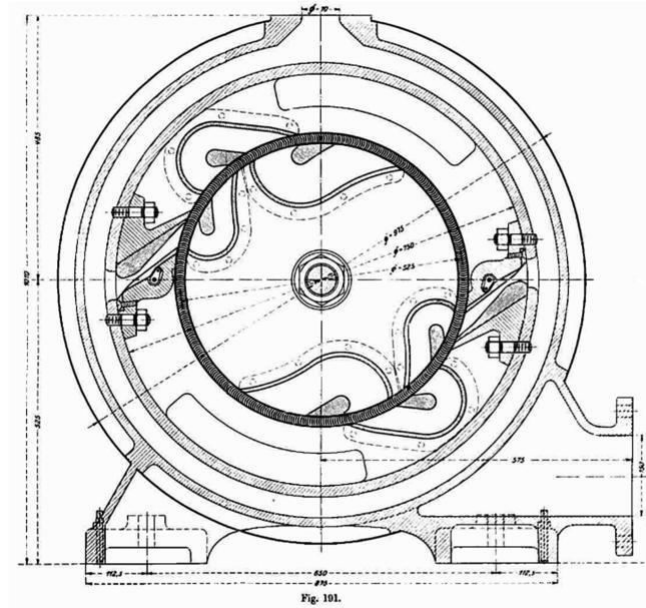


Figure 1: Example of an Elektra turbine with four wheel passes [11].

wheel passes need some space in circumferential direction. Therefore, the wheel diameter must be rather large. The multiple velocity compounding leads to rather small necessary circumferential speed, u , (see Table 2) – an Elektra with four passes works at 25% of the circumferential speed of an impulse turbine. Combined with the necessary big wheel diameter D , a very small rotational speed is implementable. Those small Elektra turbines (20–300 kW) were formerly applied on ships (see [12]) to directly drive pumps and fans at very low rotational speed (≤ 3000 rpm). The achieved efficiencies of 25–50% were rather poor but acceptable because the exhaust steam was used for pre-heating in the ship's steam system [13].

Table 2: Comparison of required optimal circumferential speed u_{opt} as a function of the number of wheel passes (i.e. velocity stages).

	Impulse turbine	Elektra 2 passes (like Curtis 2 wheel)	Elektra 3 passes (like Curtis 3 wheel)	Elektra 4 passes (like Curtis 4 wheel)
u_{opt}	$\frac{h_{\text{is}}}{2} \quad 0.5$	$\frac{1}{2} \frac{\Delta h_{\text{is}}}{2} \quad 0.5$	$\frac{1}{3} \frac{\Delta h_{\text{is}}}{2} \quad 0.5$	$\frac{1}{4} \frac{\Delta h_{\text{is}}}{2} \quad 0.5$
	100%	50%	33%	25%

The achievable very low rotational speed would nowadays allow the application of a standard 3000 rpm generator instead of the currently commonly considered high-speed generator which is rather expensive and requires an additional frequency converter. Furthermore, future decentralized small power plants will mostly provide district heating as well. Thus, the poor efficiency, i.e., the higher heat content in the exhaust steam will be used for district heating and is not necessarily a major disadvantage.

2 Methodology

Re-entry turbines were not uncommon in the beginning of the 20th century. There were different types of axial flow and radial flow re-entry turbines (see [11, 14]). Unfortunately, existing literature from this time is very scarce. The NASA (National Aeronautics and Space Administration) investigated re-entry turbines in the sixties, because they provided very high power output combined with low weight and a simple design which seemed to be advantageous to drive rocket pumps (see [15–18]). These papers only deal with axial re-entry turbines. The only recent publication known to the authors that deals with a radial re-entry turbine design is written in Polish [19]. Thus, the authors have developed their own first Elektra design approach based on the already available in-house 1D turbine design tool for axial impulse, axial Curtis, radial impulse and reaction turbines [20]. In the following, we describe the considerations, which lead to the first version of the Elektra-turbine-design-tool and our first Elektra turbine demonstrator.

The wheel or the buckets respectively can only be designed or optimized for one flow pass (diameter, diameter ratio, blade angles, blade height, number of blades, etc.). The same is valid for circumferential speed u . Hence, for the other passes, 'design' is not a design calculation but rather an analysis calculation.

Because pressure builds up from downstream to upstream, the idea is to start with exit pressure of the last wheel pass and then calculate flow velocity, velocity triangle, total and total relative thermodynamic condition at wheel exit, calculate flow velocity, velocity triangle, total and total relative thermodynamic condition at wheel inlet by assessment of enthalpy losses based on the available loss models. If there is a nozzle upstream of the wheel pass, the (supersonic) nozzle can be calculated (flow area, length) by means of a simple loss correlation for Laval nozzles [20]. The convergent-divergent nozzles show a rectangular cross-section area and the divergent

part is equipped with straight walls. The area increase is implemented only in one dimension (see Fig. 1). Such rather simple nozzles work very reliably (see [1, 20]).

If there is a deflection channel upstream of the wheel pass, the channel is designed, i.e. flow areas are calculated for constant pressure under consideration of enthalpy dissipation as function of Mach number and deflection angle like for a blade row. Because especially the deflection angle is a function of absolute inlet angle at the considered wheel pass and absolute exit angle of the wheel pass just upstream, it becomes obvious that the boundary condition of the calculation is influenced by its results. Thus, this task cannot be solved just analytically, it must be solved iteratively.

The working fluid, the inlet total conditions, the required mass flow rate and the static exit pressure must be defined to start this iterative approach. Furthermore, an expansion efficiency must be assessed to determine the static outlet conditions of the final wheel pass. An optimal circumferential velocity can be assessed by Table 2, depending on the number of wheel passes.

The turbine blade wheel is partly determined based on experience, partly designed: The outer diameter, D_{out} , is determined with respect to the desired or possible maximum rotational speed. The diameter ratio, D_{in}/D_{out} , should be close to unity (about 0.95) in order to avoid useless adding and extracting of pumping work by the centrifugal pressure field for each wheel pass. The blade angles of the impulse buckets ($\beta_{out} = 180^\circ - \beta_{in}$) should be chosen in the range $15^\circ < \beta_1 < 20^\circ$. The required blade height can then be calculated with the outlet diameter of the final wheel pass, the blade angle, the thermodynamic outlet conditions and the mass flow rate.

The outer and inner shell areas of the wheel should be equal because the flow passes the wheel from both sides, i.e. the blade height from outer to inner diameter varies inversely proportional to the wheel diameter: $h_{out}/h_{in} = D_{in}/D_{out}$.

As a result of the velocity compounding, absolute velocity and its radial component drops from wheel pass to wheel pass. Thus, the degree of admission, i.e. the flow area of the deflection channels must increase from pass to pass. Furthermore, with decreasing (radial component of) velocity, the angle between the absolute velocity, c , and circumferential velocity, u , is getting smaller, because relative flow angle, β (blade angle) and circumferential velocity, u , are fixed. Therefore, the final nozzle inclination to circumferential direction will be higher than the usual $12\text{--}15^\circ$ of classical impulse or axial Curtis turbine stages. Due to the defined constant area

wheel $A_{in} = A_{out}(\pi D_{in}h_{in} = \pi D_{out}h_{out})$ the flow would not change its relative velocity without friction. However, with friction, i.e. growing boundary layers (reducing effective flow area), for relative flow Mach numbers below unity, the flow accelerates, i.e. pressure drops. For relative Mach numbers higher than unity in contrast, the flow decelerates, i.e. the pressure rises. Thus, despite an impulse wheel design ($\beta_{out} = 180^\circ - \beta_{in}$, $A_{in} = A_{out}$), a pressure change occurs for every wheel pass. Several internal and external iterations must be performed until the required total inlet pressure is achieved for the given mass flow rate (i.e. swallowing capacity of the turbine is met) and the calculated expansion efficiency coincides with the original assessed one. Based on these considerations and assumptions, we designed our first Elektra turbine demonstrator for pressurized air which will be introduced in the flowing subsection.

Turbine design data

The Laboratory for Turbomachinery at the Technical University of Applied Sciences Amberg–Weiden is equipped with an eddy current brake for high-speed pressurized air drives. Therefore, we designed our first Elektra turbine demonstrator for pressurized air and not for steam or organic vapors. Testing with pressurized air is by far simpler than with steam and allows checking our design approach and our loss models. The Elektra design data (see Table 3) were determined corresponding to the capabilities

Table 3: Turbine main design data.

Parameter	Unit	Elektra air Turbine
Working fluid	–	pressurized air
Mass flow rate	kg/s	0.065
Total inlet pressure	kPa	1000
Total inlet temperature	K	≈ 293
Static exit pressure	kPa	≈ 100
Wheel diameter, D_{out}	m	0.08
Rotational speed, n	rpm	29 000
Degree of admission, ε	%	≈ 61
Pressure ratio, PR (ts)	–	10
Nozzle exit Mach number, Ma_1	–	2.04
Rotor relative inlet Mach number, Ma_{r1}	–	1.58
Calculated efficiency, η_{ts} (1D-tool)	%	64
Expected shaft power	kW	≈ 5

of the brake and the installed air compressors. Figure 2 displays a drawing of the Elektra turbine generators and some photographs of the parts ready for assembly.

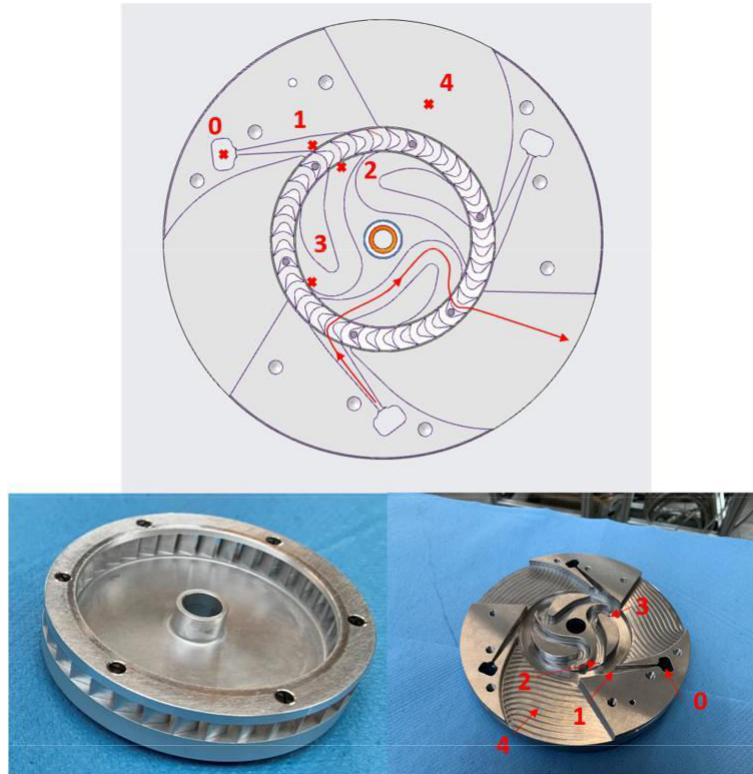


Figure 2: Drawing (top) of the Elektra turbine demonstrator featuring three Laval nozzles, three deflection channels, which allow for two wheel passes. The crosses are the locations of the pressure tapings, the arrowed line shows the flow direction. The shrouded cantilever wheel is shown in the lower left picture, the back part of the casing with the integrated nozzles and deflection channels on the lower right.

3 Numerical approach

The preliminary 1D-design the Elektra turbine was supported by means of 3D CFD-simulations. Both steady and unsteady Reynolds averaged Navier-Stokes (RANS) methods were applied using the EURANUS flow solver from NUMECA, which is incorporated in the FINE/Turbo package [21, 22]. The

governing equations to describe the prevailing flow conditions are solved in the relative frame of reference on multiblock structured grids. These equations are discretized with a cell centered control volume approach in space and with a four-stage Runge–Kutta scheme in time. For a more detailed description of the flow solver, the interested reader is referred to Hirsch *et al.* [21] and Jameson *et al.* [22].

The simulation model, displayed in Fig. 3, comprises one periodic pitch which extends over 120° for this case. Table 4 provides an overview of the corresponding boundary conditions and modelling assumptions. The Reynolds-averaged Navier–Stokes (RANS) equations are solved in conjunction with the Spalart–Allmaras turbulence model. This one – equation model requires only moderate computing resources, while still providing reliable results for complex flows in turbomachines. To further limit the computational effort, particularly for the unsteady simulations, a wall function has been applied to model the flow within the boundary layer. Thus,

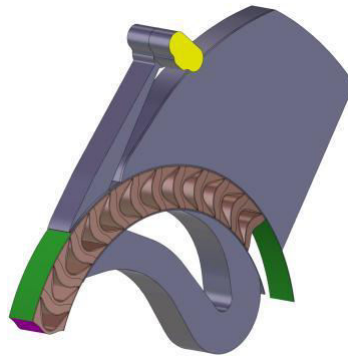


Figure 3: Simulation model (V2).

Table 4: Physical models and boundary conditions of the CFD Simulations.

Modell or condition	Parameter
Mathematical model	Turbulent Navier–Stokes
Turbulence model	Spalart–Allmaras with extended wall function
Rotor-stator interface	Full non-matching frozen rotor
Efficiency definition	Total to static isentropic
Fluid model	Air (perfect gas)
Inlet boundary condition	Absolute total pressure $p_0 = 1000$ kPa Total temperature $T_0 = 293.15$ K
Outlet boundary condition	Averaged static pressure $\bar{p}_{\text{out}} = 100$ kPa

the grid nodes next to the wall are placed within the logarithmic range of the boundary layer, rather than in the viscous sublayer. The resulting mesh contains approximately 9.5 million cells with a first cell height of 10 m. The number of nodes necessary to fully resolve the boundary layer would have been about twice as high compared to the ‘high-Re’ wall treatment. For the steady simulation, flow quantities are exchanged via a full non-matching frozen rotor interface between stationary and rotating domains. As will be shown in the next section, this approach, however, does not lead to a satisfactory agreement when compared with measurements of the global turbine efficiency. Instead, the average of an unsteady simulation must be computed, to achieve a better match. In the present paper, only the numerical results for the design point are considered, that is a total to static pressure ratio of 10 with a rotational speed of 29 000 1/min.

A first approach to numerically investigate the prevailing flow conditions in the turbine was impeded by the occurrence of backflow at the outlet during a steady state calculation. To address this issue, the outlet shape has been modified. A comparison of the original and the modified turbine, including an impression of the flow field is given by Fig. 4, which displays the radial velocity component for the original geometry in Fig. 4a and the modified model in Fig. 4b. As will be elaborated in the next section, a considerable percentage of the incoming mass flow does not enter the rotor blade passage but passes directly over the leading edge toward the outflow. The result is a large area with recirculating flow in the outflow, also leading to the backflow at the outlet. This has a negative impact on the numerical stability of the simulation model and on the credibility of the numerical results. Hence, all numerical investigations were conducted with the adapted shape of the outlet.

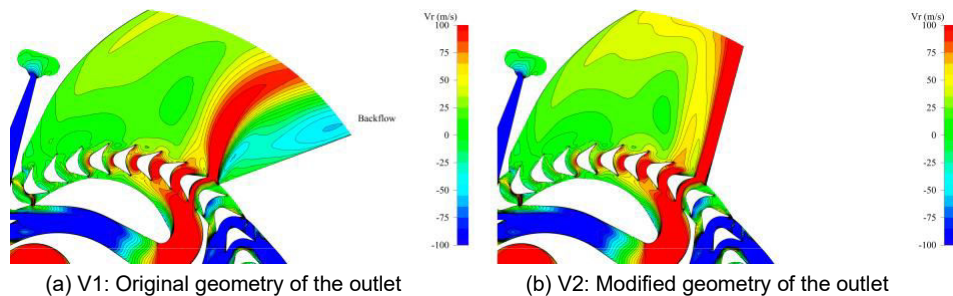


Figure 4: A contour plot illustrating the radial (absolute) velocity component for two numerical models, V1 and V2, at approximately 50% span relative to the nozzle height at the design point for a steady state solution.

4 Results

4.1 Simulation results

Figure 5 displays four representative flow quantities on a constant span position at 50% of the nozzle height. They stem from a steady state computation at design conditions. As will be shown at the end of this section, a steady simulation is only suitable to a limited extend to resolve the prevailing flow conditions. However, it provides the means to obtain a first impression of the flow dynamics and to reveal some potential for further improvements of the geometry.

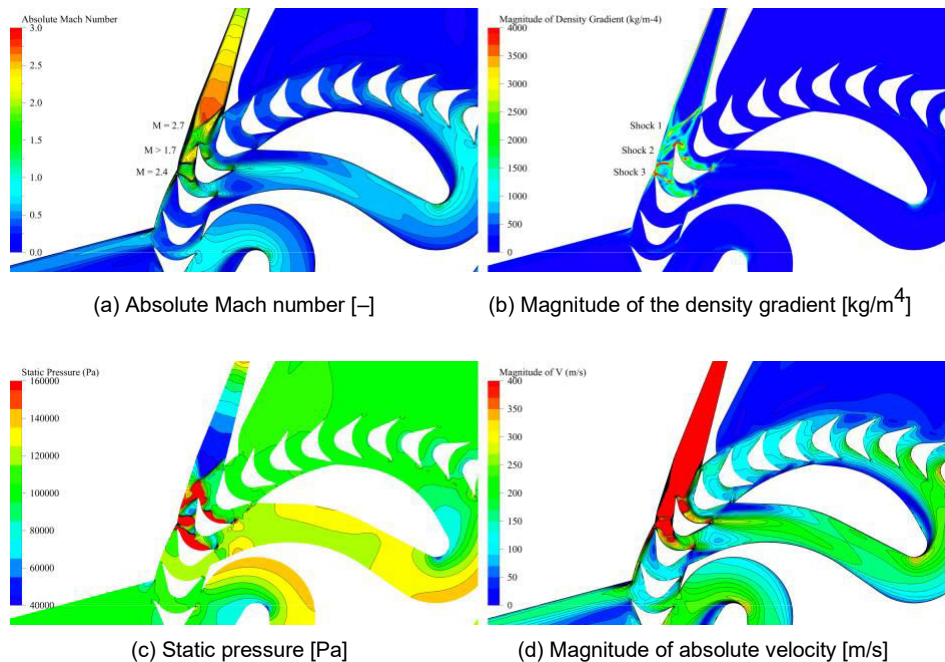


Figure 5: Different flow quantities on approximately 50% span for a steady state solution with a frozen rotor interface at design conditions.

To begin with, the reader is referred to Fig. 5a. The flow has entered the nozzle and expands through the divergent part where it reaches a maximum Mach number of approximately 2.7. The divergent part of the nozzle terminates with a sharp edge on one side and with a minor turning on the other side (the flow is turned into itself). Thus, the expansion stops momentarily with an oblique shock wave, labeled with shock 1 in Fig. 5b.

Downstream, the flow decelerates but remains supersonic. As it approaches the leading edge of the turbine wheel, the flow is divided into two parts, each experiencing different area progressions. The 'left part', relative to the view in Fig. 5a, accelerates again to a Mach number of 2.4, since the blade is forming another diverging nozzle together with the turbine casing. Ultimately, another shock wave is formed (shock 2) leading to a strong positive pressure gradient in the streamwise direction. This might cause that a considerable amount of the flow is not entering the blade passage but passes directly over the leading edge towards the outflow instead. The leakage jet becomes clearly visible by plotting the magnitude of the absolute velocity, as can be seen in Fig. 5d. This mass flow leakage is estimated to be approximately 9% of the inlet mass flow by the steady state solution. The remaining flow overcomes the turning in the turbine with another oblique shock annotated with 3. Except for a small region with flow separation on the suction side (induced by the shock waves 2 and 3), the flow remains supersonic until the blade passage diverges and guides the flow towards the deflection channel.

In this channel, the flow suffers from viscous dissipation causing a pressure loss of approximately 20 kPa. The main reason for this is twofold. First, as a result from the complex flow phenomena upstream, the flow exits the turbine with very high velocity gradients in both the circumferential and the spanwise direction. This non-uniform flow is propagated downstream which leads to an inhomogeneous flow field in the entire channel. The second reason is the significant turning of the channel in conjunction with a high ratio of the channel width to the curvature radius. The strong curvature and the associated pressure gradient normal to the inner curve leads to a very low pressure and the flow reaches sonic conditions. As a result, the flow close to the inner radius has to overcome a pressure increase from approximately 50 kPa to about 100 kPa (see Fig. 5c) before the flow enters the turbine wheel a second time. This leads to a relatively large area with flow separation, which can be clearly seen in Fig. 5d.

Complementary to the frozen-rotor approach, an unsteady Reynolds averaged Navier-Stokes (URANS) computation has been conducted to analyze the influence from highly unsteady interactions throughout in the turbine, particularly between the nozzle exit and the turbine wheel. A direct comparison reveals that the mass flow leakage is about 6 pp higher in the unsteady simulation. Hence, 9–15% of the incoming mass flow does not contribute to the energy conversion and are practically lost. Also, the total specific enthalpy drop appears to be overestimated by the steady simulation

by nearly 11%. The influence of both effects can be directly noted in the isentropic efficiency, which is predicted to be 39.8% for the unsteady case and 47.1% for the steady simulation. The measurements, which are about to be discussed in the next section, show an efficiency of approximately 33% – an offset of 7 pp compared to the unsteady average.

So, the question arises whether the area ratio of the nozzle is just too big, or the swallowing capacity of the downstream flow geometry is over-estimated by the 1D-turbine-tool (loss model)? The first hypothesis is not supported by the experience of the authors although it cannot be excluded. The second seems to be more probable, because the pressure distribution (Fig. 5c) shows a significant pressure drop and flow separation in the region of the strong flow turning which is contradictory to the ‘constant pressure design approach’ for the deflection channel.

4.2 Experimentally determined performance maps

In the following, the experimentally determined performance maps of the Elektra turbine demonstrator are presented. Figure 6 shows the measured total-to-static isentropic efficiencies for different investigated pressure ratios (CPR) as a function of the rotational speed.

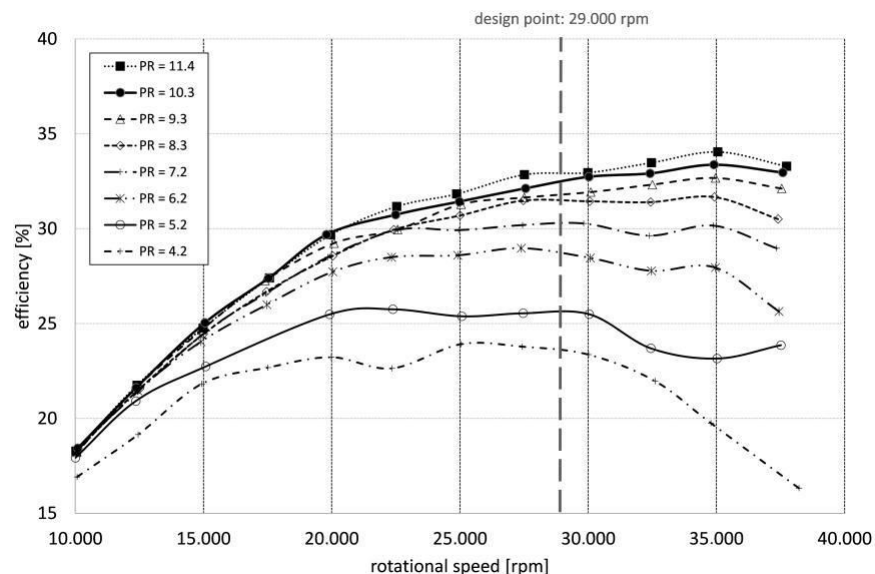


Figure 6: Total-to-static isentropic efficiency as a function of rotational speed for the different pressure ratios.

The efficiency at the design point (29 000 rpm, $PR = 10$) reaches only about 33%. This is about half of the efficiency predicted by the 1D-turbine-tool (64%) but confirms the more pessimistic results from the unsteady computational fluid dynamics (CFD) analysis (39.8%). For higher pressure ratios ($9.3 < PR < 11.4$), efficiency slightly increases for higher rotational speeds compared to the design value. For pressure ratios below, the efficiency curves are very flat and efficiency starts to drop for rotational speeds higher than 29 000 rpm. A deviation from design pressure ratio of $\pm 10\%$ does not affect the efficiency significantly. This robust behavior of the Laval nozzles is already known from other tested supersonic turbines [1, 8, 23, 24].

Figure 7 compares measured static pressures (black crosses) with numerical results along a representative extract from the flow path in the CFD-simulation. The abscissa represents the streamwise coordinate and marks limits of each turbine component, such as the end of the nozzle or the beginning of the channel. This surface is plotted with a contour plot of the static pressure at the bottom of figure. Its informative value is similar to the plots in Fig. 5. However, it emphasizes the strong variation of state variables along the spanwise direction, particularly at the end of the nozzle and during the first wheel pass. The trends for selected span-locations (hub, shroud, mid span) are diagramed above, together with the measured pressure values.

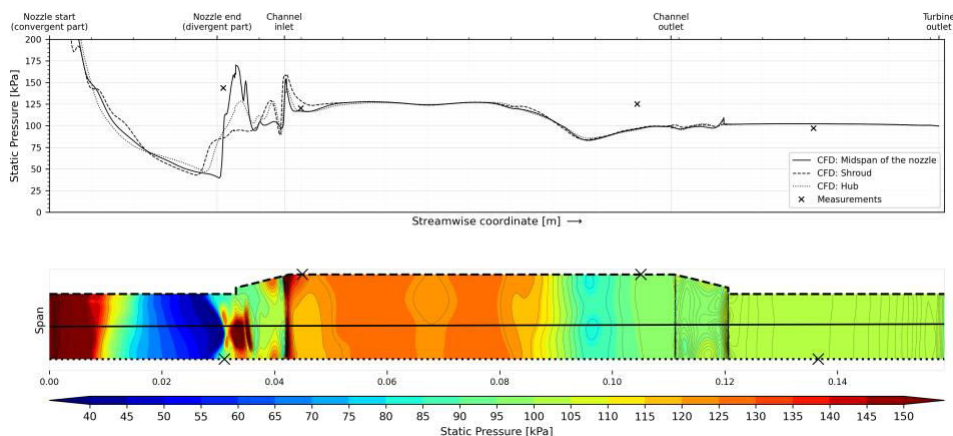


Figure 7: Development of static pressure through the Elektra turbine at design conditions. The black crosses represent locations (bottom plot) and pressure (upper plot) from measurements. The numerical results stem from the steady CFD solution.

The first measurement point is located at the hub slightly downstream of the divergent part of the nozzle. This is also where the first oblique shock wave occurs in the steady CFD solution, namely shock 1 in Fig. 5b. Accordingly, the pressure increases at all three spanwise locations. However, the agreement with the measured value is not very satisfactory when comparing it with the CFD solution at the hub. A slightly better match can be found when comparing the measured value to the trend at midspan instead. The different trends allow the conclusion that the flow is highly three-dimensional despite of the 2D-shape of the nozzle.

After the flow has undergone a series of pressure oscillations in the blade passage, it enters the deflection channel. Here, the spanwise variation is not as intense as at the previous measurement point. Accordingly, the measured value taken at the shroud agrees very well with the numerical results at this location.

As already mentioned before, the CFD calculation shows a pressure drop within the deflection channel, which the authors tried to avoid in the design by an appropriate area increase. This pressure drop is not confirmed by the 3rd measurement value. However, it should be noted that this point is located in an area (see Fig. 2 and 5c) where the pressure gradient in all directions is very high due to the significant turning of the flow in this area. Therefore, a single pressure value may not be representative for this location.

The last measurement point is centered on the hub of the outflow and is dominated by the ambient pressure which was measured to be 96.5 kPa on that day.

5 Discussion

It is obvious that the loss model in the 1D tool significantly underestimated flow dissipation. However, this loss model showed better agreement in former investigations of supersonic axial impulse, axial Curtis and radial cantilever turbines [1, 8]. Thus, probably the loss assessment for the deflection channels is too optimistic. The deflection channels were designed as constant pressure channels, i.e. the flow area increases to compensate pressure losses due to friction. However, CFD calculations determine a pressure drop by approximately 20 kPa (Fig. 5c and 7). Thus, the deflection channels must be modified. Furthermore, currently, they do not have a fixed cover. The rotating wheel builds the fourth wall of the channel. Thus, there is an additional gap, which was not modelled in the numerical simulation.

However, the leakage jet identified in the CFD calculation is the most surprising finding. The authors are convinced that this phenomenon occurs in reality as well and is responsible for at least a lack of 10 pp in efficiency. Measures must be identified, to avoid this phenomenon, such as modification e.g. of the swallowing capacity of the buckets by increasing the pitch to chord ratio or reducing area ratio of the nozzles, both in order to avoid the oblique shock with the resulting pressure rise upstream of the buckets.

6 Conclusion

In the present paper, some well-known but currently rarely applied turbine architectures are discussed and evaluated with regard to their application in future small-scale (100 kW) decentralized Rankine power stations, which convert, e.g. waste heat from combined heat and power (CHP) units or industry. It has become obvious that the concept of a velocity compounded re-entry turbine provides the potential to implement small, cost-effective turbines driving standard generators. However, this can only be reasonable, if the poor expansion efficiency is acceptable, e.g. in the case of additional condensation heat utilization.

Due to a lack of design data or design examples in literature, the authors developed their own design approach and 1D-design-tool for the so-called Elektra turbine, i.e. radial single wheel velocity compounded re-entry turbine. This Elektra demonstrator was investigated numerically and experimentally. The measured efficiencies achieved only approx. 35%, which is not acceptable for the considered application. Expansion efficiencies of at least 50% must be achieved and data of old designs show that this is possible – in particular, taking into account nowadays capabilities of computational fluid dynamics. Therefore, the authors will test different modifications of the Elektra turbine and will try to bring the 1D-design-tool closer to reality by means of the measured data.

Acknowledgments The work presented in this paper was conducted within the frame of the btha-project (jc 2018-56) “Low cost turbo expanders for decentralized energy applications – possibilities of 3d print manufacturing from modern plastic materials”. The authors want to thank the Bayerisch-Tschechische Hochschule-Agentur (btha) for their financial support.

Furthermore, the work presented in this paper was supported by the “Technologie- und Wissenschaftsnetzwerk Oberpfalz (TWO)”. The authors want to thank the TWO for their financial support.

Received 16 June 2020

References

- [1] Weiss A.P., Popp T., Müller J., Hauer J., Brüggemann D., Preissinger M.: *Experimental characterization and comparison of an axial and a cantilever micro-turbine for small-scale Organic Rankine Cycle*. Appl. Therm. Eng. **140**(2018), 235–244. DOI: [10.1016/j.applthermaleng.2018.05.033](https://doi.org/10.1016/j.applthermaleng.2018.05.033).
- [2] de Laval Carl Gustaf Patrik: *Steam Turbine*.
- [3] Weiss A.P.: *Volumetric expander versus turbine – which is the better choice for small ORC plants?* In: University of Liège and Ghent University, editor. ASME-ORC2015: Proc. 3rd Int. Seminar on ORC Power Systems; 2015.
- [4] Harris F.R.: *The Parsons centenary – a hundred years of steam turbines*. Proc. Ins. Mech. Eng., Part A: Power and Process Engineering **198**(1984), 3, 183–224.
- [5] Somerscales E.F.C.: *The Vertical Curtis steam turbine*. Trans. Newcomen Soc. **62**(1990), 1, 157–158.
- [6] Beer R.: *Aerodynamic design and estimated performance of a two-stage Curtis turbine for the liquid oxygen turbopump of the M-1 engine*. Prepared for National Aeronautics and Space Administration; 1965.
- [7] Trollheden S., Bergenlid B., Aglund A., Pettersson A.: *Development of the turbines for the Vulcain 2 turbopumps*. In: 35th Joint Propulsion Conf. Exhibit. Reston: American Institute of Aeronautics and Astronautics, 1999.
- [8] Weiss A.P., Popp T., Zinn G., Preissinger M., Brüggemann D.: *A micro-turbine-generator-construction-kit (MTG-c-kit) for small-scale waste heat recovery ORC-plants*. Energy **181**(2019), 51–55.
- [9] Macchi E., Astolfi M. (Eds.): *Organic Rankine cycle (ORC) power systems: Technologies and applications*. Woodhead Publishing is an imprint of Elsevier; Elsevier; 2017.
- [10] Klonowicz P., Fijałkowski T., Antczak Ł., Magiera R.: *Radial Curtis stage*. In: 10th Conf. on Power System Engineering, Thermodynamics & Fluid Flow: ES 2011, Pilsen 2011.
- [11] Stodola A.: *Die Dampfturbinen: Mit einem Anhang über die Aussichten der Wärmekraftmaschinen und über die Gasturbine*. Berlin, Heidelberg, s.l.: Springer, Berlin Heidelberg 1905 (in German).
- [12] Meuth H.: *The Elektra steam turbine*. J. American Soc. Naval Eng. **22**(1910), 2, 402–416.
- [13] Stodola A.: *Die Dampfturbinen: Mit einem Anhang über die Aussichten der Wärmekraftmaschinen und über die Gasturbine*. (1st Edn.) Springer, Berlin 2012 (in German).
- [14] Mewes R.: *Dampfturbinen: Deren Entwicklung, Bau, Leistung und Theorie nebst Anhang über Gas- und Dampfluftturbinen*. Salzwasser Verlag, Paderborn 2011 (in German).

- [15] Linhardt H.D.: *Study of Turbine and Turbopump Design Parameters: a Study of High Pressure Ratio Re-Entry Turbines*. Pacoima 1960.
- [16] Linhardt H.D.: *Re-entry turbines for secondary space power systems*. ARS J. **32**(1962), 10, 1552–60.
- [17] Evans D.G.: *Design and Experimental Investigation of a Three-Stage Multiple-Reentry Turbine*. NASA 1959.
- [18] Holeski D.E., Wintucky W.T.: *Experimental Investigation of a 4.54-Inch-Mean-Diameter Three-Stage Reverse-Flow Reentry Turbine*. Washington, D.C. 1963.
- [19] Kryłowicz W., Liśkiewicz G., Szwaja S.: *A design of a small steam turbine of Elektra type for a dispersed power sector*. Energetyka 2015, 11, 719–22 (in Polish).
- [20] Weiss A.P., Novotný V., Popp T., Zinn G., Kolovratník M.: *Customized small-scale ORC turbogenerators- combining a 1D-design tool, a micro-turbine-generator-construction-kit and potentials of 3D-printing*. In: Proc. 5th Int. Seminar on ORC Power Systems ORC2019, The National Technical University of Athens, 2019.
- [21] Hirsch C., Lacor C., Rizzi A., Eliasson P., Lindblad I., Haeuser J.: *A multi-block/multigrid code for the efficient solution of complex 3D Navier–Stokes flows*. ESA, Aerothermodynamics for Space Vehicles: Proc. First European Symposium, ESTEC, Noordwijk, 28–30 May 1991, 415–420.
- [22] Jameson A., Schmidt W., Turkel E.: *Numerical solution of the Euler equations by finite volume methods using Runge Kutta time stepping schemes*. In: Proc. 14th Fluid and Plasma Dynamics Conf. Reston, Virigina: American Institute of Aeronautics and Astronautics; 06231981.
- [23] Weiss A.P., Zinn G.: *Micro turbine generators for waste heat recovery and compressed air energy storage*. In: Proc. 15th Conf. on Power System Engineering, Thermodynamics & Fluid Flow: ES 2016. 978-80-261-0626-5, 2016.
- [24] Weiss A.P., Hauer J., Popp T., Preissinger M.: *Experimental investigation of a supersonic micro turbine running with hexamethyldisiloxane*. In: Proc. 16th Conf. on Power System Engineering, Thermodynamics & Fluid Flow: PSE 2017. AIP Publ. 2017, 20050.